Coherent control of vibrational transitions: Discriminating molecules in mixtures

A. C. W. van Rhijn, A. Jafarpour, M. Jurna, H. L. Offerhaus and J. L. Herek

Received 13th March 2011, Accepted 11th May 2011
DOI: 10.1039/c1fd00040c

Identifying complex molecules often entails detection of multiple vibrational resonances, especially in the case of mixtures. Phase shaping of broadband pump and probe pulses allows for the coherent superposition of several resonances, such that specific molecules can be detected directly and with high selectivity. Our particular implementation of coherent anti-Stokes Raman scattering (CARS) spectroscopy and imaging employs broadband pump and probe fields in combination with a narrowband Stokes field. We describe our approach for combining spectral phase shaping and closed-loop optimization strategies to perform chemically-selective microscopy. To predict the optimal excitation profile we employ evolutionary algorithms that use the vibrational phase responses of five distinct molecules with overlapping resonances and investigate the effect of phase instability on the optimization. We have recently shown that modified polynomials and orthogonal rational functions can give rise to improved contours for CARS fitness landscapes. Now, by considering the landscapes associated with different basis sets, we introduce two figures of merit to quantitatively rank basis functions in terms of their "appropriateness" for modeling nonlinear phase-shaped processes.

Introduction

Coherent anti-Stokes Raman scattering (CARS) has been used successfully in spectroscopy and microscopy since the development of (tunable) pulsed laser sources.[1] In CARS, molecular vibrations are excited coherently by a combination of a pump (ω_p) and Stokes (ω_s) pulse. Subsequently, a probe (ω_{pr}) pulse, which is often derived from the same pulse as the pump, generates the anti-Stokes (CARS) signal ($\omega_c = \omega_p - \omega_s + \omega_{pr}$). By obtaining its contrast from molecular vibrations, CARS is a label-free imaging technique.

A vibrational resonance can be considered as a damped driven harmonic oscillator with a certain resonance frequency, resonance strength, and damping factor. The response of such a harmonic oscillator yields a peak in the amplitude spectrum and a phase step from 0 to $-\pi$ in the phase response at the resonance frequency. As multiple resonances are combined, the peaks in the amplitude spectrum add up linearly, but the phase responses combine in such a way that the phase remains between 0 and $-\pi$. The vibrational phase of the resonances can be used to suppress non-resonant contributions to the CARS signal.[2]

Here we show how phase-shaped pulses that specifically address the vibrational phase of the molecules can be used to enhance desired CARS signals and simultaneously suppress non-resonant contributions. To predict optimal response functions

Optical Sciences group, MESA+ Institute for Nanotechnology, Faculty of Science and Technology (TNW), University of Twente, The Netherlands

we employ evolutionary strategies that use the vibrational phase responses of five distinct molecules with overlapping resonances. We first address the basic concepts and then report the following new contributions: 1) extension of phase-shaped CARS strategy to a larger library of mixtures, 2) a coherence sensitivity analysis to quantify the negative contribution of parameters such as the jitter (between pump and Stokes beams) and phase noise on the performance of these optimizations, and 3) quantitative ranking of basis sets in terms of their "appropriateness" for modeling a phase-shaped CARS process.

1. Phase-shaped CARS

Introduction

Although successful, narrowband CARS (Fig. 1(a)) has disadvantages, such as the need for a unique identifying spectral feature to identify a constituent in a mixture of resonant compounds and its need for a tunable laser source to access different vibrations. Broadband CARS, where one or more of the input pulses are broadband (femtosecond) pulses,[3,4] especially in combination with pulse shaping,[5–11] can circumvent these problems.

Our approach is based on a double broadband interaction, where the degenerate pump and probe pulses are broadband and the Stokes pulse is narrowband (Fig. 1 (b)). Due to this double broadband interaction there are many different combinations of pump and probe wavelengths which lead to the same wavelength CARS signal. Even though the CARS wavelength is the same for these combinations, the vibrational frequency that is addressed is different for each combination, leading to a difference in amplitude and phase of the CARS signal, giving rise to interference. We can influence this interference by changing the spectral phase profile of our pump and probe pulses. We previously reported on an intuitive shaping strategy, based on mimicking the π-phase step of a vibrational resonance.[12,13] Using more complex phase shapes, further control over the CARS signal is possible, but in order to accurately calculate the CARS signal that is generated by such phase shaped pulses, detailed knowledge of the vibrational response (including the phase information) is needed.

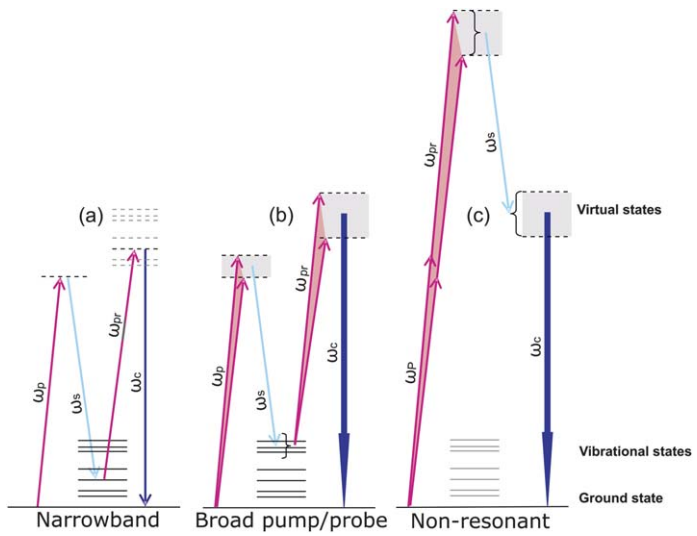

Fig. 1 Energy level diagram for (a) narrowband CARS, (b) broadband pump and probe CARS, and (c) non-resonant four-wave mixing.

The vibrational phase response

The vibrational phase response can be measured directly using heterodyne detection[14] or vibrational phase contrast CARS.[15] Several other indirect techniques exist that retrieve the vibrational phase from a recorded broadband CARS spectrum.[16–19] Here, we determine the vibrational phase response by fitting with an evolutionary algorithm[20] of the spontaneous Raman scattering spectrum.[21,22] The spontaneous Raman spectrum corresponds to the negative imaginary part of the individual vibrational lineshapes (eqn (1)). By fitting the negative imaginary part of a sum of vibrational lineshapes to the spontaneous Raman spectrum, the vibrational phase can be retrieved. We employ a covariance matrix adaptation evolution strategy (CMA-ES)[23] to solve the fitting problem. Details of the code implementing CMA-ES are reported elsewhere.[24] An example fit for polystyrene is shown in Fig. 2(a,b).

$$I_{\mathrm{Raman}}(\omega) \propto -\Im[\chi^{(3)}(\omega)] = -\Im[\chi^{(3)}_{\mathrm{NR}} + \sum_{\mathrm{R}} \frac{A_{\mathrm{R}}}{(\omega_{\mathrm{R}}^2 - \omega^2 + 2i\omega\gamma_{\mathrm{R}})}] \quad (1)$$

Pulse optimization

Using the complete vibrational response to calculate the CARS signal, CMA-ES is used to numerically optimize the spectral phase of the pump (=probe) pulse. The CMA-ES optimizes the spectral phase $\phi(\omega)$ of the pump and probe pulses such that the difference in CARS signal, integrated over the full bandwidth, generated by a pump- and probe-pulse with phase $\phi(\omega)$ and a pump- and probe-pulse with phase $-\phi(\omega)$ is maximized. By subtracting the CARS signals generated by a phase profile $\phi(\omega)$ and its inverse $-\phi(\omega)$, the purely non-resonant background is removed.[12,13] Using the difference as the target for the optimization yields a phase profile that enhances the desired molecule's response, while suppressing other contributions.

The pump (and probe) pulse is assumed to have a Gaussian spectral power distribution with a center wavelength of 806.5 nm (12400 cm^{-1}) and a FWHM of 26 nm (400 cm^{-1}). The Stokes pulse is assumed to have an infinitely small bandwith with a center wavelength of 1064.3 nm (9395.85 cm^{-1}). The spectral phase profile is optimized by the CMA-ES on 40 points, divided evenly over 1021 cm^{-1}. This phase profile is extended to 4096 points by cubic spline interpolation in order to improve the resolution when calculating the CARS response. The CMA algorithm uses 20 parents and a population size of 40 per generation. The non-resonant background is assumed to be constant with a ratio between resonant and non-resonant response of 5 : 1 (peak to baseline). An example of an optimized phase profile for maximum signal from pure polystyrene is shown in Fig. 2(c). The shape of the excitation profile clearly reflects the molecular phase response 2(b), as the optimal pulse compensates the phase profile of the molecule. Optimizations with different ratios of

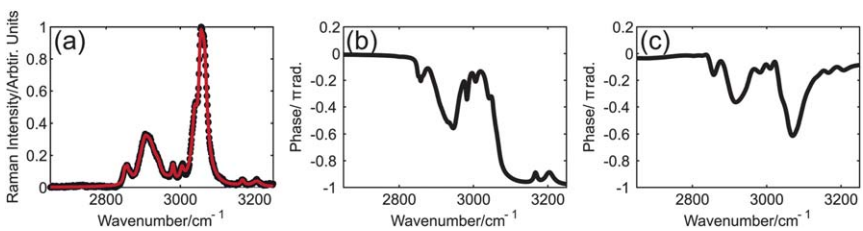

Fig. 2 (a) Spontaneous Raman spectrum (black) and fit (red) of polystyrene and (b) retrieved vibrational phase. Panel (c) shows the optimal excitation phase for maximum CARS signal from polystyrene.

non-resonant background showed similar results, as the purely non-resonant signal is discarded by looking at the difference CARS signal. The mixing between resonant and non-resonant signal influences the depth of the phase jumps in the optimized phase, but the general shape remains the same.

Besides optimizing the phase for maximum signal from a compound, it is also possible to optimize for minimum signal. Combining these two ideas, it is possible to optimize the excitation phase for selective excitation of a single constituent in a mixture of resonant compounds.[22] Here, we consider a mixture of five resonant compounds; polystyrene, PMMA, polyethene, toluene, and ethanol. These five substances have strongly overlapping resonances in the region around 3000 cm^{-1}, which is accessed by our combination of input pulses (pump-Stokes). Using CMA-ES, we calculate five different excitation phases that selectively excite one of the resonant compounds, while minimizing the contributions from the other four compounds. An example of such a selective excitation phase for optimizing the CARS signal from polyethene is shown in Fig. 3. The complicated spectral phase pattern (red curve) that results from the optimization bears little resemblance to the vibrational phase profile of polyethene (black curve). Fig. 3(b) shows the corresponding learning curve, truncated after 400 generations to better illustrate how contributions from the other molecules are actively suppressed. After 1000 generations, the CARS signal from polyethene in the mixture reaches a contrast ratio of 500 : 1. Remarkably, the signal is diminished by only 30% relative to the optimized signal for the pure substance. The obtained results and contrast ratios for all five substances can be found in Table 1.

It can be seen from Table 1 that the contrast and total signal is lowest for polystyrene and toluene. These two molecules have very similar chemical structures, and hence the vibrational response is also very similar. Therefore, it is more difficult to differentiate between the two and the obtained contrast ratio and total signal is lower. It should be noted that the obtainable contrast ratio might be lower if multiple resonant compounds are present in the focal volume simultaneously. This potential decrease in contrast ratio is due to homodyne mixing of the CARS signals in the focal volume.[22]

Effect of noise

In order to gain insight into the robustness of this optimization approach under laboratory constraints, we consider the effect of noise on the optimization process. We simulate fluctuations caused by, for example, the spatial light modulator or jitter between the different laser sources by adding a random phase noise to each point of the phase pattern that is simulated. The resulting phase profiles are described by

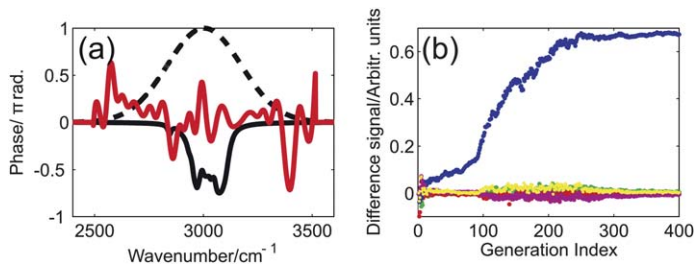

Fig. 3 (a) Optimized excitation phase (red) for maximum signal from polyethene and minimum signal from PMMA, polystyrene, toluene and ethanol. Furthermore, the pump (=probe) pulse envelope (dotted black line) and the vibrational phase of polyethene (solid black line) is shown. (b) Integrated difference CARS signals as a function of generation of the CMA algorithm for polystyrene (green), PMMA (red), polyethene (blue), toluene (yellow), and ethanol (magenta).

Table 1 CARS signal and contrast ratios for selective excitation of a single compound in a mixture of 5 resonant compounds. The first column indicates the optimized compound and the cells of that row show the amount of integrated difference CARS signal normalized to the amount of signal obtained from a pure sample of the optimized compound with a pulse optimized for its maximum signal

Compound	Polystyrene	PMMA	Polyethene	Toluene	Ethanol	Contrast
Polystyrene	0.05	$< 4 \times 10^{-4}$	$< 4 \times 10^{-4}$	$< 4 \times 10^{-4}$	$< 4 \times 10^{-4}$	132 : 1
PMMA	$< 3 \times 10^{-4}$	0.66	$< 3 \times 10^{-4}$	$< 3 \times 10^{-4}$	$< 3 \times 10^{-4}$	2200 : 1
Polyethene	$< 1.5 \times 10^{-3}$	$< 1 \times 10^{-3}$	0.71	$< 1.5 \times 10^{-3}$	$< 1.5 \times 10^{-3}$	470 : 1
Toluene	$< 6 \times 10^{-4}$	$< 2 \times 10^{-4}$	$< 2 \times 10^{-4}$	0.10	$< 4 \times 10^{-4}$	168 : 1
Ethanol	$< 1 \times 10^{-3}$	$< 1 \times 10^{-3}$	$< 1 \times 10^{-3}$	$< 1 \times 10^{-3}$	0.42	415 : 1

$\phi_{\text{total}} = \phi_{\text{orig}} + \Phi_{\text{noise}} n(\omega)$, where ϕ_{orig} denotes the original (noiseless) phase pattern, Φ_{noise} is a scaling factor for the noise level (in radians), and $n(\omega)$ is a random sequence of noise values with a uniform distribution between -1 and 1. The obtained contrast ratio and CARS signals for different levels of noise strength are presented in Table 2.

Table 2 shows the devastating role of phase instability on these coherent processes by a decrease of the contrast ratio from 470 : 1 to 5 : 1, corresponding to a noise span of $\Phi_{\text{noise}} = 0$ to $\Phi_{\text{noise}} = 0.5\pi$. This effect can be compared and correlated with the smear out of coherent control landscapes, as shown in[25] (see Fig. 11 therein). With a given level and type of hardware noise, alternative formulations, such as delay-based pulse shaping,[26] are expected to provide some (software-based) noise robustness and maintain reasonably high contrast ratios.

Comparing previous experimental results based on control with a π-phase step[13] with the noise model presented in Table 2, we attribute an effective noise level of $\Phi \approx 0.23\pi$ as a rough estimation of noise in our previous experiment.

2. Quantitative ranking of basis sets

Introduction

Identification and ranking of an "appropriate" set of basis functions to describe a (nonlinear) pulse shaping problem is one of the key questions in both open- and closed-loop coherent control. In linear operator theory, this is a well-established classical problem. By considering functions as generalized vectors in an inifinite-dimensional (Hilbert) space, an appropriate basis set (of eigenfunctions) can be considered as the independent (orthogonal) axes of the space. Such eigenfunction decompositions have been successfully used in quantitative and intuitive

Table 2 CARS signal and contrast ratios for selective excitation of polyethene in the presence of various levels of noise. The normalized signal is once again relative to the signal obtained from a pure sample of polyethene with a pulse optimized for maximum signal from polyethene

Noise Level	Contrast Ratio	Norm. CARS signal
0	470 : 1	0.71
0.01π	300 : 1	0.71
0.02π	79 : 1	0.71
0.05π	47 : 1	0.71
0.1π	28 : 1	0.71
0.2π	14 : 1	0.56
0.5π	5 : 1	0.07

formulation of problems such as wavepacket dynamics in molecules and light propagation in optical fibers with both fundamental and practical significance.

Our motivation for finding alternative basis sets for pulse shaping spectroscopy is to create an intuitive approach that is easily applicable to experiments. As such, we have recently suggested the relative convex shape of contours in the energy landscape as a measure of "appropriateness" of a basis set. For a real non-degenerate linear operator with orthonormal eigenfunctions Ψ_n and a unity weight function, an arbitrary function f can be written as $f = \sum c_n \Psi_n$. According to Parsevall's theorem, the (statistical) energy of the function f can be described as $E_f = \sum c_n$, which is the equation of a hyper-sphere. This is the ideal optimization landscape, as the contours $E = E_n$ are symmetric, isotropic, convex (see Fig. 4), connected, and without relative rotation.[25] With the convex contour as a qualitative figure of merit, we have shown the superiority of orthogonal rational functions for a third-order resonant process[27] and modified polynomials for a second-order non-resonant process.[25] However, these comparisons have been done by visual inspection and in a qualitative way. Here, we report on two figures of merit that can be used for quantitative and automated comparison of different basis sets in spaces with arbitrary dimensionalities.

First figure of merit: isoperimetric quotient

A closed string will enclose the largest area when it is stretched uniformly to form a circle. This intuitive property, referred to as the isoperimetric inequality in a more formal terminology, is the basis of our approach. Also note that any concave shape can be modified towards a convex shape with the same circumference, but a larger area, by "flipping the dents" (see Fig. 4(C)). So, if P and A denote the circumference and the area of a closed shape, the ranking factor $IPQ = 4\pi A/P^2$ (referred to as the isoperimetric quotient) ranks convex shapes on top of "comparable" concave ones (see Fig. 4(C)) and a circle on top of all convex shapes; which is exactly what we are looking for. The IPQ can also be expressed in three- and higher-dimensional spaces, where visual inspection is difficult or even impossible. It is specifically useful for the automated global search of weight factors in Gram–Schmidt-like modifications of a basis set[25] in high-dimensional spaces. Note that the search for such alternative bases does not require new simulations or measurements, except possibly for improving the resolution.[25]

While the IPQ is a useful figure of merit to evaluate the convex shape and the apparent ellipticity of a contour, it can yield similar values for a concave contour and an elongated convex one. A complementary figure of merit is one that only

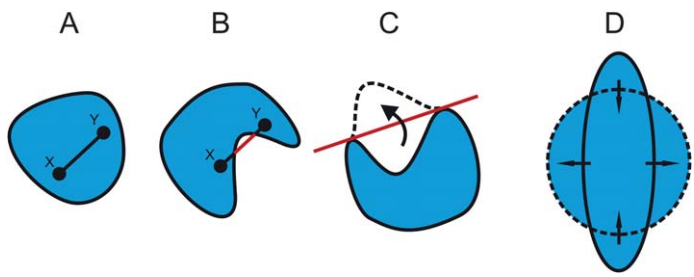

Fig. 4 (A) A convex curve; the line segment connecting any two arbitrary points within the enclosed area will lie entirely within the enclosed area. (B) A concave curve; the line segment connecting at least one pair of points within the enclosed area will lie partially outside the enclosed area. (C) By "flipping a dent", it is possible to convert a concave shape to a convex one with the same circumference, but a larger area. (D) Among convex patterns with the same circumference, a circle encloses the largest area.

differentiates between convex and concave contours with no sensitivity to the elongation of convex contours.

Second figure of merit: convex hull quotient

When a stretched elastic band encompassing an object is released, it is (partially) attached to a cross section of the object. The resulting shape of the released band is referred to as the convex hull (minimal convex set) of the cross section. If the cross section is convex, the convex hull is the cross section itself. The difference between the areas enclosed by a contour and its convex hull is a measure of deviation from a convex shape. We define a second figure of merit, referred to as Convex Hull Quotient (CHQ), to be the ratio of the areas enclosed by a contour and its convex hull. CHQ is a figure of merit complementary to the IPQ. For CHQ values (considerably) smaller than unity, the contours have (considerable) deviation from a convex shape. If the CHQ is (close to) one, then the IPQ is (mainly) a measure of elongation of a convex contour.

Quantitative comparison of basis sets

We have recently shown how the choice of an appropriate basis set can lead to landscapes with visibly smoother, more convex contour lines, for a given CARS configuration.[27] Here we compare the CARS landscapes associated with polynomial and Kautz bases[27] (quantitatively), using the IPQ and CHQ figures of merit introduced in this contribution. All simulation parameters are the same as provided in ref. 27.

The number of data points along each coordinate is chosen to be 200 in order to have a reasonably small numerical error in discretization of contours with small areas. The first analyzed contour corresponds to 88% of the maximum fitness, which has been discretized with 35 points along the periphery. The last analyzed contour corresponds to 39% of the maximum fitness, and has been discretized with 245 points. It corresponds to the lowest fitness, for which the contour in the polynomial landscape is completely accommodated in appropriately-chosen range of the landscape.[27] Further numerical considerations are beyond the scope of this contribution, and will be addressed separately.

As seen in Fig. 5, the contours in the polynomial landscape deviate more from a convex shape (lower IPQ), as the fitness drops (compared to the contours in the other landscape). A higher value of IPQ for a given contour level implies more insensitivity to the direction approaching the contour. From a practical perspective, if a laser setup starts from similar energy levels, but different initial (background) phase every day, the optimizations will remain essentially repeatable, and also take approximately the same amount of time. Also note that if the contours of a landscape are obtained from each other by isotropic scaling, then the IPQ will be a constant function of contour level (almost similar to Fig. 5, bottom right). While the convex (concave) shape of contours in the Kautz (polynomial) landscape is noticeable by visual inspection in Fig. 5(A) and 5(B), the same information is quantitatively demonstrated using the aforementioned figures of merit in Fig. 5(C) and 5(D). The value of this approach will be especially apparent when comparing multiple solution landscapes generated by a variety of basis functions.

Summary and discussion

We have shown the feasibility of using an evolutionary algorithm to extract vibrational phase information from spontaneous Raman scattering data and using this information to optimize broadband coherent anti-Stokes Raman scattering (CARS). By optimizing the spectral phase profile of our broadband pump (=probe) pulse we can obtain selective excitation of a single compound in a mixture of resonant compounds. We predict contrast ratios ranging from 170 : 1 to 2200 : 1 for each separate compound in a mixture of five compounds. The obtained contrast

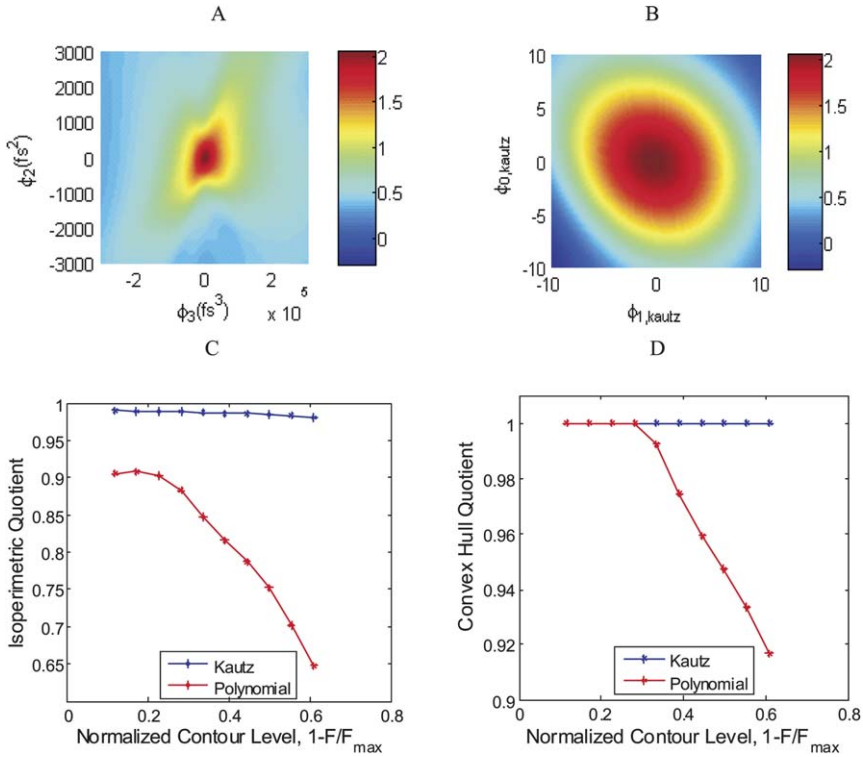

Fig. 5 Two-dimensional landscapes of the CARS process with (A) polynomials and (B) Kautz functions, and (C) isoperimetric quotient and (D) the convex hull quotient values, associated with the contours in both landscapes.

ratio depends on the uniqueness of the complex vibrational response of the molecule of interest compared to that of the surrounding molecules. In the presence of phase noise an optimal phase profile can still be found, but the obtainable contrast ratio will decrease as the noise level increases. Furthermore we have shown the advantages of considering alternative basis sets and we have introduced a method of quantitatively ranking these basis sets based on the isoperimetric quotient and the convex hull quotient.

The results of this study have both fundamental and practical implications for coherent control:

• A fundamental question in spectroscopy with shaped pulses is the nature of the control mechanism.[28] Enchancing the CARS signal generated in our experiments can be achieved by either a transform limited pulse or a pulse that compensates the phase of the vibrational resonance. In practice, an optimization seeks a compromise to these two effects (see section 2.2 of ref. 27). As such, the optimal solutions of CARS signals from a mixture are not only about a trade-off between the signals of individual compounds, but also about a compromise between competing mechanisms in each compound.

• The strategies discussed in this paper all fall in the category where the temporal dynamics of the excited vibrational states do not play a direct role. A first step toward control where the dynamics are directly addressed would be to include the effects of vibrational relaxation and create pulses that excite one vibrational level and probe another level at some later time.

• While the employed technology is relatively new, the notion of using temporal interferences of all resonances (rather than a spectral scan of individual resonances)

is a familiar concept in vibrational spectroscopy. One may consider phase-shaped CARS a nonlinear generalization (or analogue) of FTIR or FT-Raman spectroscopy.

• In general, evaluation of the IPQ and the CHQ of different contour lines (geometrical changes) should be done along with an explicit verification of local optima or lack thereof (possible topological changes). Regarding the two specific cases of polynomials and Kautz functions, this issue has been addressed in Section 6.4 of ref. 27.

Acknowledgements

This research is supported by the Stichting voor Fundamenteel Onderzoek der Materie (FOM, grant number 03TF78-3), which is supported financially by Nederlandse Organisatie voor Wetenschappelijk Onderzoek (NWO). This work is also supported by the IOP (Innovatiegerichte Onderzoeksprogramma's) Photonic Devices program managed by the Technology Foundation STW (Stichting Technische Wetenschappen) and AgentschapNL.

References

1 P. D. Maker and R. W. Terhune, *Phys. Rev. Lett.*, 1965, **137**, A801.
2 E. O. Potma, C. L. Evans and X. S. Xie, *Opt. Lett.*, 2006, **31**, 241.
3 H. Kano and H. Hamaguchi, *Opt. Express*, 2005, **13**, 1322.
4 G. W. H. Wurpel, J. M. Schins and M. Müller, *J. Phys. Chem. B*, 2004, **108**, 3400.
5 D. Oron, N. Dudovich and Y. Silberberg, *Phys. Rev. Lett.*, 2002, **89**, 273001.
6 D. Oron, N. Dudovich and Y. Silberberg, *Phys. Rev. A: At., Mol., Opt. Phys.*, 2004, **70**, 023415.
7 S. O. Konorov, X. G. Xu, J. W. Hepburn and V. Milner, *Phys. Rev. A: At., Mol., Opt. Phys.*, 2009, **79**, 031801.
8 V. V. Lozovoy, B. Xu, J. C. Shane and M. Dantus, *Phys. Rev. A: At., Mol., Opt. Phys.*, 2006, **74**, 041805.
9 J. Konradi, A. K. Singh and A. Materny, *Phys. Chem. Chem. Phys.*, 2005, **7**, 3574.
10 J. Konradi, A. Scaria, V. Namboodiri and A. Materny, *J. Raman Spectrosc.*, 2007, **38**, 1006.
11 S. D. McGrane, R. J. Scharff, M. Greenfield and D. S. Moore, *New J. Phys.*, 2009, **11**, 105047.
12 S. Postma, A. C. W. van Rhijn, J. P. Korterik, P. Gross, J. L. Herek and H. L. Offerhaus, *Opt. Express*, 2008, **16**, 7985.
13 A. C. W. van Rhijn, S. Postma, J. P. Korterik, J. L. Herek and H. L. Offerhaus, *J. Opt. Soc. Am. B*, 2009, **26**, 559.
14 M. Jurna, J. P. Korterik, C. Otto, J. L. Herek and H. L. Offerhaus, *Opt. Express*, 2008, **16**, 15863.
15 M. Jurna, J. P. Korterik, C. Otto, J. L. Herek and H. L. Offerhaus, *Phys. Rev. Lett.*, 2009, **103**, 043905.
16 S. H. Lim, A. G. Caster, O. Nicolet and S. R. Leone, *J. Phys. Chem. B*, 2006, **110**, 5196.
17 S. H. Lim, A. G. Caster and S. R. Leone, *Opt. Lett.*, 2007, **32**, 1332.
18 E. M. Vartiainen, H. A. Rinia, M. Müller and M. Bonn, *Opt. Express*, 2006, **14**, 3622.
19 Y. Liu, Y. J. Lee and M. T. Cicerone, *Opt. Lett.*, 2009, **34**, 1363.
20 W. L. Meerts and M. Schmitt, *Int. Rev. Phys. Chem.*, 2006, **25**, 353.
21 M. H. Hennessy and A. M. Kelley, *Phys. Chem. Chem. Phys.*, 2004, **6**, 1085.
22 A. C. W. van Rhijn, M. Jurna, A. Jafarpour, J. L. Herek and H. L. Offerhaus, *J. Raman Spectrosc.*, 2011, DOI: 10.1002/jrs.2922.
23 N. Hansen, "The CMA evolution strategy: a tutorial" http://www.lri.fr/∼ hansen/cmatutorial.pdf, 2010 description.
24 R. Fanciulli, L. Willmes, J. Savolainen, P. van der Walle, T. Bäck and J. L. Herek, *Lect. Notes Comput. Sci.*, 2008, **4926**, 219.
25 P. van der Walle, H. L. Offerhaus, J. L. Herek and A. Jafarpour, *Opt. Express*, 2010, **18**, 973.
26 D. Yang, D. P. Sprünken, A. C. W. van Rhijn, J. Savolainen, T. L. Chen, H. L. Offerhaus, J. L. Herek and A. Jafarpour, *Opt. Commun.*, 2011, **284**, 2748.
27 A. C. W. van Rhijn, H. L. Offerhaus, P. van der Walle, J. L. Herek and A. Jafarpour, *Opt. Express*, 2010, **18**, 2695.
28 T. Brixner, N. H. Damrauer, B. Kiefer and G. Gerber, *J. Chem. Phys.*, 2003, **118**, 3692.